Chlorine in wadsleyite and ringwoodite: An experimental study

Mathilde Roberge, Hélène Bureau, Nathalie Bolfan-Casanova, Caroline
Raepsaet, Suzy Surble, Hicham Khodja, Anne-Line Auzende, Patrick Cordier,
Guillaume Fiquet

Chlorine in wadsleyite and ringwoodite: an experimental study

Mathilde Roberge[1], Hélène Bureau[1], Nathalie Bolfan-Casanova[2], Caroline Raepsaet[3],

Suzy Surble[3], Hicham Khodja[3], Anne-Line Auzende[4], Patrick Cordier[5], Guillaume

Fiquet[1].

[1] Institut de Minéralogie, de Physique des Matériaux et de Cosmochimie (IMPMC), Sorbonne

Universités – UPMC Univ. Paris 06, CNRS UMR 7590, Muséum National d'Histoire Naturelle, IRD

UR 206, 4 place Jussieu, 75252 Paris Cedex 05, France

[2] Laboratoire Magmas et Volcans, Université Blaise Pascal, Clermont-Ferrand, France

[3] LEEL, NIMBE, CEA, CNRS, Université Paris-Saclay, CEA Saclay, 91191 Gif-sur-Yvette Cedex,

France

[4] Université Grenoble Alpes, ISTerre, UMR5275 F-38041 Grenoble cedex 9, France

[5] UMET Lille

For submission to *Earth and Planetary Sciences Letters*

Corresponding author : Hélène Bureau

e-mail : helene.bureau@impmc.upmc.fr

24   Abstract
25
26
27

28   We report concentrations of Chlorine (Cl) in synthetic wadsleyite (Wd) and ringwoodite

29   (Rw) in the system $NaCl-(Mg,Fe)_2SiO_4$ under hydrous and anhydrous conditions. Multi-anvil

30   press experiments were performed under pressures (14-22 GPa) and temperatures (1100-

31   1400°C) relevant to the transition zone (TZ: 410-670 km depth). Cl and H contents were

32   measured using Particle Induced X-ray Emission (PIXE) and Elastic Recoil Detection Analysis

33   (ERDA) respectively. Results show that Cl content in Rw and Wd is significantly higher than

34   in other nominally anhydrous minerals from the upper mantle (olivine, pyroxene, garnet), with

35   up to 490 ppm Cl in anhydrous Rw, and from 174 to 200 ppm Cl in hydrous Wd and up to 113

36   ppm Cl in hydrous Rw.

37   These results put constrains on the Cl budget of the deep Earth. Based on these results,

38   we propose that the TZ may be a major repository for major halogen elements in the mantle,

39   where Cl may be concentrated together with H_2O and F (see Roberge et al., 2015). Assuming

40   a continuous supply by subduction and a water-rich TZ, we use the concentrations measured in

41   Wd (174 ppm Cl) and in Rw (106 ppm Cl) and we obtain a maximum value for the Cl budget

42   for the bulk silicate Earth (BSE) of 15.1×10^{22} g Cl, equivalent to 37 ppm Cl. This value is larger

43   than the 17 ppm Cl proposed previously by McDonough and Sun (1995) and evidences that the

44   Cl content of the mantle may be higher than previously thought. Comparison of the present

45   results with the budget calculated for F (Roberge et al., 2015) shows that while both elements

46   abundances are probably underestimated for the bulk silicate Earth, their relative abundances

47   are preserved. The BSE is too rich in F with respect to heavy halogen elements to be compatible

48   with a primordial origin from chondrites CI-like (carbonaceous chondrites CC) material only.

49   We thus propose a combination of two processes to explain these relative abundances: a

50   primordial contribution of different chondritic-like materials, including EC-like (enstatite

51   chondrites), possibly followed by a distinct fractionation of F during the Earth differentiation

52   due to its lithophile behaviour compared to Cl, Br and I.

53

1. Introduction

Halogen elements (fluorine F, chlorine Cl, bromine Br, iodine I) are minor volatiles compared to hydrogen and carbon. Major halogens F and Cl have been mostly studied for their role in the shallowest Earth's reservoirs: lithosphere, crust, atmosphere, and hydrosphere, mostly because they are the most abundant halogens and because they have been shown to be strongly involved in volcanic and igneous processes. Indeed, Cl is an important constituent of volcanic fumaroles and plumes, and form individualized fluids such as brines and molten salts. These brines are strongly involved in hydrothermal systems and in ore forming processes (see the reviews after Pyle and Mather 2009; Shinohara 2009; Aiuppa et al., 2009). Cl is particularly used to trace igneous processes and ore-forming processes, and to track magmas from their genesis to their eruption Cl is known to affect magma properties (see Pyle and Mather, 2009), it is significantly degassed from subaerial volcanic activity (e.g. Aiuppa, 2009), and it can impact the stratosphere chemistry. Cl is enriched in sea water, it has been shown that oceanic subduction delivers fluids to the mantle through serpentinites related processes (serpentinization and deserpentinization), that are significantly Cl-rich (e.g. Ito et al., 1983; John et al., 2011; Kendrick et al., 2011), making this last one an important constituent in mantle metasomatism processes, that enriches the sources for arc magmatism (e.g. Tatsumi, 1989, Philippot et al., 1998; Scambelluri et al., 2004). Indeed magmas from subduction zones are among the most enriched in Cl (Ito et al., 1983; Straub and Layne, 2003; Kendrick et al., 2012).

During subduction, the interaction between seawater and rocks produces secondary minerals containing significant amounts of Cl (Ito et al., 1983; Pagé et al., 2016). It has thus been proposed that the subduction of oceanic lithospheric material at convergent plate boundaries would drive an annual global flux of 2.9-22 x 10^{12} g Cl to the Earth's interior (John et al., 2011). It has also been proposed that a part of the subducted Cl would reach high depths in the mantle (>200 km) and would possibly enrich the sources for Ocean Island Basalts (Kendrick et al., 2015; Joachim et al., 2015). Cl is significantly present in ultrahigh pressure metamorphic rocks (Scambelluri et al., 2004; Ottolini and Fèvre, 2008; Pagé et al., 2016), in kimberlites (Kamenetsky et al., 2004), and in inclusions of saline brines in diamonds (Weiss et al., 2014). Recent studies show that Cl is present in olivine, pyroxene, and garnet: the highest contents of Cl are measured in minerals formed by metamorphic dehydration of serpentine, olivines and pyroxenes (up to 400 ppm Cl, Scambelluri et al., 2004; Ottolini and Fèvre, 2008). In natural upper mantle nominally anhydrous minerals, the Cl contents are very low: up to 6.3 ppm in

87 olivine (Beyer et al., 2012). Partitioning experiments performed for natural compositions

88 however demonstrate the capability of upper mantle minerals to be the Cl carriers: up to 148

89 ppm Cl in orthopyroxene, 17 ppm Cl in clinopyroxene, 13 ppm in garnet, 5 ppm in plagioclase,

90 up to 170 ppm in olivine (Dalou et al., 2012). To our knowledge, there is currently no evidence

91 about the presence of Cl in the transition zone and in the lower mantle. Recently we have

92 suggested that a strong link connects the water global cycle and that of fluorine at depth

93 (Crepisson et al., 2014; Roberge et al., 2015). We have proposed that the transition zone can be

94 a major reservoir for fluorine (Roberge et al., 2015). It could be similar for Cl.

95 This study aims at constraining the possible deep storage and cycling of Cl through the

96 determination of Cl potential contents in wadsleyite (Wd) and ringwoodite (Rw), the major

97 minerals of the transition zone (TZ). We use these data to discuss the Cl content of the bulk

98 silicate Earth.

99

100 ## 2. Materials and methods

101

102 ### 2.1. Starting materials an experimental strategy

103 The starting bulk composition was olivine Fo_{90} with a slight excess of silica ((Mg+Fe)/Si atomic

104 ratio =1.75), obtained with a mixture of (1) oxide powders of MgO, SiO_2, FeO, or (2) natural

105 Fo_{90} olivine with SiO_2 powder. 5 wt% of Cl was added to the mixture as crushed NaCl powder.

106 NaCl was chosen as the source of Cl because it is enriched in sea water and in subducted oceanic

107 floor. For experiments under hydrous conditions, 2wt% of water was added as brucite

108 $Mg(OH)_2$, an amount close to the expected water solubility in wadsleyite and ringwoodite in

109 the transition zone. Samples were synthesized in multi-anvil presses at LMV Clermont-Ferrand

110 (France) and at the Bayerisches Geoinstitut of Bayreuth (Germany) following the procedure

111 described in Frost et al. (2001) and Demouchy et al. (2005). Experiments were performed from

112 14 to 22 GPa and from 1100°C to 1400°C during 0.5 to 9 hours, (Table 1). The samples were

113 enclosed in Re, Pt or Au-Pd capsules. Temperatures were monitored with W3Re/W25Re

114 thermocouples located at the top of the capsules. After the run, the experiments were quenched

115 by switching off the electric power before decompression.

116

117 ### 2.2. Sample characterization

118 The mineral assemblages were recovered, embedded in epoxy and mirror polished on one side.

119 They were analyzed with Raman spectroscopy and scanning electron microscopy at first. The

textures were investigated with a Zeiss Ultra 55 field emission scanning electron microscope (SEM) equipped with an Energy Dispersive X-Ray spectroscopy (EDX) system. Major elements compositions of wadsleyites and ringwoodites were subsequently measured by Electron Probe Micro Analysis (EPMA) on CAMECA-SX100 at CAMPARIS facility (UPMC, France). For these quantitative analyses, we used an acceleration voltage of 15 kV and a beam current of 10 nA with an 15 µm defocused beam.

A thin section of ringwoodite sample was prepared with a Focus Ion Beam (FIB), using a gallium beam with a FEI Strata DB 235 at IEMN (Lille France). A transmission Electron Microscopy (TEM) study was performed on this FIB section at UMET, Lille (France) with a FEI Tecnai G2-20 twin operating at 200 kV.

Chlorine and hydrogen contents were measured using ion beam analysis, Particle Induced X-Ray Emission (PIXE) for Cl and Elastic Recoil Detection Analysis (ERDA) for H at the nuclear microprobe of the Laboratoire d'Etude des Eléments Légers (LEEL), CEA Saclay. Cl concentrations of the mineral phases Wd and Rw were obtained using incident beams of 3*3 µm^2 mapped on large areas (50*50 to 200*20 µm^2). The procedure is detailed in (Bureau et al., 2010; 2015). We used different incident beams (H$^+$ and ^{4}He$^+$ from 1.7 to 3 MeV) in order to control the depth of investigation in the samples. With mineral phases a few tens of µm in size embedded in a quenched Cl-Si-rich glass (present at grain boundaries), compromise had to be found between energy and detection in order to avoid any chlorine contribution from glassy phase. Indeed the depths investigated by the ion beams depend both on the nature of the incident ion (H$^+$, ^{4}He$^+$) and on the energy of the beam, (*i.e.* the highest the energy is the deepest is the investigation). For a San Carlos olivine, the depth of analysis for a proton beam is 50 µm at 3 MeV and 25 µm at 1.7 MeV. For one given energy, this depth is reduced when the incident ion is heavier than H$^+$, at 2 MeV the investigated depth of ^{4}He$^+$ is 6 µm.

Hydrogen (i.e. water) contents of Rw and Wd were measured using ERDA. We used a 3 MeV ^{4}He$^+$ beam, following the protocol described in Raepsaet et al. (2008), Bureau et al. (2009) and Withers et al. (2012). Simultaneous Cl analysis were also performed by PIXE during ERDA. We scanned the beam on selected areas of the sample (from 30x30 to 150x100 µm^2). Durations of analysis were chosen from 1800 to 7200 seconds. ERDA and PIXE were associated to simultaneous Rutherford Backscattering Spectrometry (RBS) measurements used to monitor the cumulated charge delivered to the sample during the acquisition (see Bureau et al., 2009). They also provided information on the matrix chemical composition of the samples. For all ion beam analysis, the software RISMIN (Daudin et al., 2003) was used to process the data by selecting the areas of interest in the chemical maps (see Fig. 1). It was particularly useful for

154 the detection of NaCl-rich glasses (grain boundaries, cracks or surface contamination), which

155 would affect H and Cl contents. Once the areas were selected, ERDA spectra were processed

156 by using SIMNRA (Mayer et al., 1997) and PIXE spectra were processed by using the

157 GUPIXWIN software (Campbell et al., 2000). Analysis were cross-checked against: NIST

158 SRM610 glass (Rocholl et al., 1997), KE12 (pantellerite lava from Kenya, Metrich and

159 Rutherford, 1992), EtC3 (Cl-Br-I-bearing $NaAlSi_3O_8$ glass, Bureau et al., 2000). The sensitivity

160 (i.e. detection limit) with respect to Cl was of a few tens of ppm (30-40 at maximum) depending

161 on the conditions (beam energy, grain size, size of the selected areas).

162

163

164 **3. Results**

165

166 **3.1. Synthesized samples**

167

168 Ten samples were synthesized (see Table 1). Among these samples, two are volatile-free (no

169 H_2O and no Cl), two are anhydrous (Cl-enriched but no H_2O), and six are Cl-H_2O-enriched.

170 Recovered mineralogical assemblages are described in Table 1. They correspond to the mineral

171 assemblages expected for the pressure and temperature conditions of the transition zone. The

172 minerals are in equilibrium with a saline and silica-rich melts mostly present at grain

173 boundaries. SEM shows that wadsleyite and ringwoodite phases exhibit subhedral or euhedral

174 shapes and various crystal sizes (Fig. 1 and 2). In the runs performed at 14 GPa, we observe

175 enstatite in agreement with literature (Inoue 1994; Inoue et al. 1995; Bolfan-Casanova 2000).

176 For runs performed at 22 GPa, stishovite ($\sim$10 μm in size) is found in equilibrium with

177 ringwoodite (50-300 μm in size Fig. 2). For all experiments, crystals are embedded in a Si-Na-

178 Cl-rich interstitial glass at grain boundaries which corresponds to the residual melt. No

179 particular textural differences or abrupt increase in the relative proportion amount of quenched

180 glasses are noted between experiments performed at different temperatures. Optical observation

181 and SEM measurements show that the crystals are pure, inclusion-free ringwoodites and

182 wadsleyites (no visible inclusions). Furthermore, a 100 nm thickness lamella of ringwoodite

183 (sample #S5553) was studied by transmission electron microscopy TEM (Figure 3). No Cl-rich

184 or NaCl-rich micro or nano-inclusions have been observed.

185   EMPA analyses show that the Cl-bearing wadsleyites and ringwoodites exhibit a Mg# ratio

186   (Mg#=Mg/(Mg+Fe) atomic ratio) ranging from 0.90 to 0.92 (Table 1 and 2), similar to the

187   Earth's mantle mineral assemblage.

188

189   **3.2**. **Chemical Characterization**

190

191   PIXE and ERDA mapping of large areas of the samples show that there is no chemical zoning

192   with respect to Cl and H in the Rw and Wd crystals. About 5 to 20 % in volume of NaCl-rich

193   glasses are present in grain boundaries (Fig. 1). Enstatite is present at 5-10% volume in all the

194   samples containing wadsleyite and stishovite is present at about 5-15% volume in all the

195   samples containing ringwoodite. A comparison between the different Cl contents obtained from

196   each analytical conditions (3 and 1.7 MeV, H^+ and He^+ beams) shows that detection limits and

197   uncertainties for Cl are dependent on the energy and ion source used (Table 2). The analyses

198   performed with a 3 MeV proton beam are the most sensitive to Cl contents but also to potential

199   contamination (Cl-rich glasses located at grain boundary) because the depth of investigation is

200   of about 50 µm. This depth is reduced to 25 µm for a beam of 1.7 MeV, and to a few µm for a

201   ^{4}He+ beam of 3 MeV, but these two last conditions are much less sensitive. As the Cl contents

202   determined at 3 MeV were systematically higher than the measurements performed at 1.7 MeV

203   with a beam of H^+ or at 2 MeV with a beam of $^4He^+$, we have only considered the measurements

204   performed at 1.7 MeV with a beam of H^+ and at 2 and 3 MeV with a beam of $^4He^+$. The lowest

205   Cl content analysed was of 60 ppm, a value higher than the detection limit. Two samples could

206   not be analysed for Cl due to the very small size of the crystals.

207   Results show that Cl contents are significant, and range from 60 ± 60 to 200 ± 48ppm Cl for

208   Wd and from 99 ± 12 to 490 ±33 ppm Cl for Rw. Anhydrous Rw contain more Cl than hydrous

209   Rw, with a maximum of 490 ppm Cl. Unfortunately, we failed analysing Cl in anhydrous Wd

210   because crystals were too small. Cl contents of hydrous Wd are ranging from 60 ± 60 to 200 ±

211   48 ppm Cl with corresponding water contents ranging from 917 ± 15 to 1659 ± 14 ppm H_2O.

212   Cl contents of hydrous Rw are ranging from 99 ± 12 to 490 ±33 ppm Cl for water contents

213   from 932 ± 14 to 4766 ± 13 ppm H_2O.

214   No relationship is observed between the temperature and both Cl and H_2O contents (i.e. OH

215   contents expressed as water equivalent concentrations, see Fig. 4 and 5). A slight decrease of

216   Cl content with pressure may be suggested for hydrous samples. The incorporation of Cl in

217   anhydrous Rw is higher than in hydrous Rw (Fig. 4 and 5). No significant dependency is found

218   between the Cl content and Mg#, FeO, SiO_2 or (Mg+Fe)/Si atomic ratio.

219   The water contents determined in Wd and Rw from this study (from 917 to 4766 ppm wt. H_2O)

220   are about one order of magnitude lower than the previously observed solubility values from the

221   literature (Bolfan-Casanova et al., 2000, Inoue et al., 1995, Demouchy et al., 2005) that reached

222   3 to 2.2 wt. % respectively, at similar temperatures. In regard to the low Cl concentrations, we

223   may exclude a competition between OH^- and Cl^- to enter in Wd and Rw structures. The

224   significant reduction of OH incorporation cannot be compensated by an exchange between OH^-

225   and Cl^-. Similar low water contents have been found in NaF-doped wadsleyite and ringwoodite

226   (Roberge et al., 2015). One sample: #40_Cl, has been synthesized together with sample #40_F

227   from this previous study. This suggests that the same process could lower water content in Rw

228   and Wd for both F and Cl-bearing samples.

229   We propose the sodium salts NaCl as NaF to be responsible of this behaviour (see Roberge et

230   al., 2015). A coupled incorporation mechanism of Na^+ and H^+ in both F and Cl-rich Wd and

231   Rw may be responsible of the low water content rather than a competitive effect between

232   halogen elements and hydroxyl groups (Roberge et al., 2015). Stalder et al. (2008) have

233   reported a strong decrease of hydrogen incorporation in pure synthetic enstatite at 2.5 GPa,

234   1150-1400°C, and shown to be a function of the NaCl added in the starting materials. The low

235   concentration of OH in enstatite is explained by a reduction of water activity in the fluid phase

236   (melt or aqueous fluid) due to the presence of dissolved salt. In our experiments, the low water

237   and possibly Cl content of the samples may be due to partitioning reaction between Rw and Wd

238   and the Si-water and NaCl-rich melt (up to 20% in volume) in equilibrium with the minerals

239   during the experiments. If true, the Cl concentrations cannot be considered as solubilities. It

240   would also explain why the water contents are so low (4766 ppm wt% at maximum) compared

241   to the initial amount of water (about 2 wt.%). Additional partitioning experiments involving a

242   Mg-rich peridotitic melt would be necessary to validate this hypothesis. As a first assumption,

243   we will consider that the Cl contents measured in Wd and Rw are corresponding to the

244   maximum contents expected in Wd and Rw in a transition zone where interstitial melt may be

245   present (e.g. Toffelmier et Tyburczy, 2007; Schmandt et al. 2014).

246

247   **3.3 Cl versus F in ringwoodite and wadsleyite**

248

249   A comparison between Cl contents (this study) and comparable F contents in Rw and Wd

250   (Roberge et al., 2015) at conditions relevant to the transition zone is presented in figure 6. All

251   the samples are comparable as we have used alternatively NaF or NaCl salts as starting

252   materials, and the same pressure and temperature conditions. We observe that Cl contents are

lower than F contents by a factor of 3 in anhydrous ringwoodites. For hydrous Rw and Wd it is more variable, as Cl contents are ranging from 60 ± 60 to 200 ± 48 ppm when F contents vary from 186 ± 19 to 850 ± 85 ppm. The difference between F and Cl solubility's in such chemical systems may reflect the difference in ionic size between F^- and Cl^-. It is likely F and OH share the same sites in olivine (Ol), wadsleyite and ringwoodite (Crepisson et al., 2014; Roberge et al., 2015), but this seems more unlikely for Cl which is larger than F and OH (Cl^- 181 nm, OH^- 140 nm). Fluorine incorporation in Ol, Wd, Rd is shown to be related to water incorporation (Crépisson et al., 2014, Roberge et al., 2015), but this is unclear for Cl. Indeed, similar Cl contents are observed in two samples of Rw with different water contents (Fig. 4). Further studies (i.e. FTIR spectroscopy) would be necessary to investigate into this direction. It is difficult to determine where Cl is incorporated in the crystal structure. The presence of OH defects in wadsleyite (Wd) and ringwoodite (Rw) have been investigated by coupling experimental observations to the modelling of infrared spectra (e.g, Blanchard et al. 2009; Blanchard et al., 2013) and provided insights into the crystal chemistry of OH in these minerals. The incorporation of Cl in Rw and Wd could be indirectly determined by studying the spectral signature of hydroxyl defects in NAMs, as for F-bearing hydrous olivines (Crépisson et al., 2014). As a first hypothesis, we suggest that in Wd and Rw, Cl, F and OH may occupy similar sites in the lattice, possibly mostly in association with Mg vacancies (as shown by Blanchard et al., 2013).

To summarize our major results: (1) the concentration of Cl in Wd and Rw is significant and can amount 490 ppm; (2) the concentration of Cl in Wd and Rw is 3 times smaller than compared to the concentration of F in the same phases synthesized in similar conditions; (3) anhydrous Rw are richer in both Cl and F than hydrous Rw; (4) the presence of water is not a pre-requisite to store Cl and F in these minerals. When present, water content is small, Cl and F contents may not be considered as solubility values for Wd and Rw, but would rather reflect partitioning reactions with an interstitial melt.

4. Discussion

4.1 Cl storage in the mantle Transition Zone's wadsleyite and ringwoodite phases

It is now recognized that the TZ is hydrated at least locally as shown by recent studies: (1) the significant water content of a hydrous ringwoodite trapped in a natural diamond exhumed from

287 the transition zone (Pearson et al., 2014), (2) geophysical data (e.g. Huang et al., 2005). We

288 consider hydrous Wd and Rw in the following sections: according to our measurements,

289 ringwoodite contains 60 ± 60 ppm Cl and 917 ± 15 ppm H_2O; wadsleyite can take up to $200 \pm$

290 48 ppm Cl and 1115 ± 14 ppm H_2O. Such significant amounts are not surprising if we compare

291 with the incorporation of fluorine in Wd and Rw (665 to 1045 ppm F, up to 956 ppm H_2O in

292 Wd and 186 to 1235 ppm F, up to 1404 ppm H_2O in Rw, see Roberge et al., 2015). Furthermore,

293 the range of water contents measured in Cl-rich Rw and Wd are consistent with what is

294 predicted for the transition zone i.e. 1000-2000 ppm (Huang et al., 2005) and 2000 ppm – 2

295 wt.% (Bercovici and Karato, 2003).

296 We assume, that no significant amounts of Cl are dissolved in the other minor mineral phases

297 of the TZ. We use an average pyrolitic composition with modal abundances of 60%wt.

298 wadsleyite from 410 to 520 km and 60%wt. ringwoodite from 520 to 660 km with addition of

299 40%wt. of garnet and clinopyroxene from 410 to 660 km (Ringwood, 1975), and with the Cl

300 contents of hydrous Fo90 wadsleyite and ringwoodite (174 ppm and 106 ppm respectively).

301 An upper bound for Cl storage in the transition zone would be of 3×10^{22}g Cl, corresponding to

302 80 ppm Cl. Wd and the Rw could be major carriers of the deep Cl, and should be thus taken

303 into account for the Earth budget of this element.

304 In order to explain a chemical contrast between low water contents in the upper mantle with

305 about 142 ppm water (Saal et al., 2002) and assuming a water-rich transition zone (having 0.2-

306 2% wt% water), Bercovici and Karato (2003) have proposed the transition zone water-filter

307 model. In this model, the downwelling fluxes driven by slabs into the transition zone and deeper

308 lower mantle trigger a passive upwelling flow. At 410 km, this upwelling flow would rises out

309 of the high-water-solubility transition zone with the transition of Wd to olivine together with a

310 water release, as olivine has a lower solubility with respect to water than Wd (Bolfan-Casanova

311 et al., 2000). Such a phase transition would then favour the formation of a melt layer overlying

312 the transition zone, having a density higher than the solid phase. This layer would act as a filter,

313 and would maintain a chemical contrast for trace and volatile elements between a depleted

314 upper mantle and an enriched upper transition zone (Bercovici and Karato, 2003), it would

315 permit a significant storage of Cl, F and H_2O in the transition zone.

316

317

318 **4.2 How much Cl in the Bulk Silicate Earth?**

319

320   Based on the average Cl contents in Mid Ocean Ridge Basalts, McDonough and Sun (1995)

321   have estimated an abundance of 17 ppm Cl for the bulk silicate Earth. We have calculated the

322   maximum Cl storage of the bulk silicate Earth, by adding the Cl contribution for each reservoir.

323   Results are summarized in the figure 7, for Cl (this study) and for F (Roberge et al., 2015).

324   For the shallow reservoirs we assume the Cl crust contribution (ocean, evaporite, brine and

325   crustal rock abundances) to be 5.8×10^{22} g (Sharp et al., 2013); we have used the value of 1 ppm

326   Cl from Saal et al., (2002) to represent the depleted shallow upper mantle. For the transition

327   zone, we assumed a hydrous TZ enriched in Cl, due to a continuous supply by subduction, we

328   obtained a maximum storage of 3×10^{22} g of Cl, corresponding to the average concentration of

329   80 ppm. For the lower mantle we used the value of 21 ppm Cl calculated from Ocean Island

330   Basalts compositions by Kovalenko et al. (2006), assumed to be representative of the primitive

331   mantle. The resulting Bulk silicate Earth content for chlorine would then be of 15×10^{22} g,

332   corresponding to a value of 37 ppm Cl, with a contribution of 20% from the transition zone

333   (Figure 7). No significant change of the F/Cl ratio is observed (0.68, McDonough and Sun,

334   1995, 0.62, this study).

335   This estimate of 37 ppm Cl in the bulk silicate Earth is twice the previous one of 17 ppm

336   (McDonough and Sun, 1995), it shows that the Earth's budget of Cl and F could be largely

337   underestimated.

338

339

340   **4.5 What about the origin of chlorine and fluorine of the Earth?**

341

342   The origin of the volatile elements for the Earth is still highly debated today, but most of the

343   models (e.g. Albarède, 2009; Javoy et al., 2010; Marty et al., 2012) propose that they originated

344   from a cosmochemical reservoir that also sourced the parent bodies of primitive meteorites.

345   The absence of correct condensation temperatures (Lodders, 2003) for both Cl and F makes

346   difficult the calculation of the predicted abundances for Cl and F in an Earth accreted from any

347   chondritic materials. For water, a chondritic origin is preferred because the terrestrial and

348   chondritic D/H ratios are similar (see Marty and Yokochi, 2006 and references therein). Among

349   the primitive meteorites, carbonaceous chondrites CC are the most popular candidates to reflect

350   the Earth's volatile source. Marty (2012) shows that a later contribution of 2±1% of

351   carbonaceous chondrite from the CI species to a dry proto-Earth would be consistent with the

352   Earth atmophile elements (C, H, N, noble gases) and is in agreement with heavy halogen

353   elements (Cl, Br, I) contents determined by McDonough and Sun (1995). However, according

354   to Marty (2012), a contribution of 17% of CI would be necessary to explain the F abundance

355   from McDonough and Sun (1995). A greater halogen content such as the one presented here

356   cannot be easily reconciled with an Earth only built by homogeneous accretion of CI

357   carbonaceous chondrite material. Alternatively, enstatite chondrites (EC) are F-enriched (i.e.

358   F/Cl = 2.77 to 1.16, Rubin and Choi, 2009), with a heavy halogen element content similar to

359   those of CI (Rubin and Choi, 2009). EC were already proposed to be the building material for

360   the Earth (e.g. Javoy, 1995), based on the isotopic signature of oxygen and nitrogen. However,

361   EC are water-poor, the Earth's Si isotopic compositions cannot be explained from a core-

362   formation scenario from a BSE having a EC's composition, and the Mg/Si ratio of the upper

363   mantle differs too much from the EC's. It is also proposed that the Earth was built from the

364   mixing of a number of chondritic like end-members having different volatile compositions

365   (Marty and Yokochi, 2006), including EC. The mixing of different volatile-rich late veneers is

366   however not sufficient to explain the depletion of Cl (and also Br and I) compared to F of the

367   BSE, which may reflect processes that have occurred during differentiation, after volatile

368   acquisition (primitive or from a late veneer). Fluorine has a lithophile character compared to

369   Cl, Br, I (McDonough and Sun, 1995). F content is greater than Cl content in both Wd and Rw.

370   During the magma ocean crystallization, F could have been stored in mantle minerals whereas

371   the heavier halogen elements may have been partially lost from the magma by devolatilization,

372   a loss possibly due to their hydrophilic affinity (Sharp and Draper, 2013; Bureau et al., 2015).

373   As long as the actual Cl and F budget of the Earth will remain un-determined, the origin of

374   volatile elements of the Earth will remain an open question.

375

376

377   **CONCLUSION**

378

379   The experimental determination of the Cl concentration in hydrous wadsleyite and ringwoodite

380   shows that they can be major carriers for Cl in the deep Earth. The transition zone can thus be

381   a deep significant repository for Cl. Cl contents are lower by a factor of 3 than those observed

382   by Roberge et al. (2015) for F. For both Cl and F, the presence of water lowers their

383   concentrations in Rw and Wd, but this storage capacity remains significant. It is thus likely that

384   both halogen elements are stored with water in the Earth's transition zone with a maximum

385   content of 80 ppm Cl.

386   Nominally anhydrous minerals are the main Cl carriers in the mantle at least down to 660 km

387   depth. Although it has been shown that F is strongly associated to water through incorporation

mechanisms in the NAMs, Cl incorporation in silicate minerals lattice is not so clear and would deserve to be further studied. Assuming a continuous supply from subduction recycling, we calculate a maximum BSE content for chlorine of 15×10^{22} g Cl, corresponding to 37 ppm Cl is proposed. The corresponding global budget for Cl is twice the value proposed by McDonough and Sun (1995). In the light of these experimental results for both Cl and F, we propose that the modern relative abundances of Cl and F may result from the combination of two processes during the Earth's accretion: a mixing contribution of CC and EC chondritic-like materials (required to generate the F enrichment compared to Cl, Br, I); possibly followed by a fractionation of F from other halogen elements during the Earth's differentiation, whereas most of the F being stored in mantle minerals when part of the heavy halogens would have been preferentially partitioned in the magma ocean, degassed and lost.

424

425

REFERENCES

Aiuppa, A., Baker, D.R., and Webster, J.D. (2009). Halogens in volcanic systems. Chem. Geol. *263*, 1–18.

Albarède F. (2009) Volatile accretion history of the terrestrial planets and dynamic implications, Nature, vol. 461, no 7268, p. 1227-1233.

Bercovici, D., and Karato, S. (2003). Whole-mantle convection and the transition-zone water filter. Nature *425*, 39–44.

Beyer, C., Klemme, S., Wiedenbeck, M., Stracke, A., and Vollmer, C. (2012). Fluorine in nominally fluorine-free mantle minerals: Experimental partitioning of F between olivine, orthopyroxene and silicate melts with implications for magmatic processes. Earth Planet. Sci. Lett. *337–338*, 1–9.

Blanchard, M., Balan, E., and Wright, K. (2009). Incorporation of water in iron-free ringwoodite: A first-principles study. Am. Mineral. *94*, 83–89.

Blanchard, M., Roberge, M., Balan, E., Fiquet, G., and Bureau, H. (2013). Infrared signatures of OH-defects in wadsleyite: A first-principles study. Am. Mineral. *98*, 2132–2143.

Bolfan-Casanova, N., Keppler, H., and Rubie, D.C. (2000). Water partitioning between nominally anhydrous minerals in the MgO–SiO2–H2O system up to 24 GPa: implications for the distribution of water in the Earth's mantle. Earth Planet. Sci. Lett. *182*, 209–221.

Bureau, H., Keppler, H., Métrich, N. (2000) Volcanic degassing of bromine and iodine : experimental fluid/melt partitioning data and applications to stratospheric chemistry, Earth and Planetary Science Letters, 183, 51-60.

Bureau, H., Raepsaet, C., Khodja, H., Carraro, A., and Aubaud, C. (2009). Determination of hydrogen content in geological. samples using elastic recoil detection analysis (ERDA). Geochim. Cosmochim. Acta *73*, 3311–3322.

Bureau, H., Auzende, A.-L., Marocchi, M., Raepsaet, C., Munsch, P., Testemale, D., Mézouar, M., Kubsky, S., Carrière, M., Ricolleau, A., Fiquet, G. (2015) The Volcanic degassing of Iodine, Geochimica et Cosmochimica Acta, 173, 114-125.

Campbell, J.L., Hopman, T.L., Maxwell, J.A., and Nejedly, Z. (2000). The Guelph PIXE software package III: Alternative proton database. Nucl. Instrum. Methods Phys. Res. Sect. B Beam Interact. Mater. At. *170*, 193–204.

Crépisson, C., Blanchard, M., Bureau, H., Sanloup, C., Withers, A.C., Khodja, H., Surblé, S., Raepsaet, C., Béneut, K., Leroy, C., et al. (2014). Clumped fluoride-hydroxyl defects in forsterite: Implications for the upper-mantle. Earth Planet. Sci. Lett. *390*, 287–295.

Dalou, C., Koga, K.T., Shimizu, N., Boulon, J., and Devidal, J.-L. (2012). Experimental determination of F and Cl partitioning between lherzolite and basaltic melt. Contrib. Mineral. Petrol. *163*, 591–609.

464 Daudin, L., Khodja, H., and Gallien, J.-P. (2003). Development of "position–charge–time"
465 tagged spectrometry for ion beam microanalysis. Nucl. Instrum. Methods Phys. Res. Sect. B
466 Beam Interact. Mater. At. *210*, 153–158.

467 Demouchy, S., Deloule, E., Frost, D.J., and Keppler, H. (2005). Pressure and temperature-
468 dependence of water solubility in Fe-free wadsleyite. Am. Mineral. *90*, 1084–1091.

469 Frost, D.J., Langenhorst, F., van Aken, P.A. (2001). Fe-Mg partitioning between ringwoodite
470 and magnesiowüstite and the effect of pressure, temperature and oxygen fugacity. Phys.
471 Chem. Minerals 28, 455-470.
472
473 Huang, X., Xu, Y., and Karato, S. (2005). Water content in the transition zone from electrical
474 conductivity of wadsleyite and ringwoodite. Nature *434*, 746–749.

475 Ito, E., Harris, D.M., and Anderson Jr., A.T. (1983). Alteration of oceanic crust and geologic
476 cycling of chlorine and water. Geochim. Cosmochim. Acta *47*, 1613–1624.

477 Javoy, M. (1995). The integral enstatite chondrite model of the Earth. Geophys. Res. Lett. *22*,
478 2219–2222.

479 Joachim, B., Pawley, A., Lyon, I.C., Marquardt, K., Henkel, T. Clay, P.L., Ruzié, L., Burgess,
480 R., Ballentine, C.J. (2015) Experimental partitioning of F and Cl between olivine,
481 orthopyroxene and silicate melt at Earth's mantle conditions. Chem. Geol. 416, 65-78.

482 John, T., Scambelluri, M., Frische, M., Barnes, J.D., and Bach, W. (2011). Dehydration of
483 subducting serpentinite: Implications for halogen mobility in subduction zones and the deep
484 halogen cycle. Earth Planet. Sci. Lett. *308*, 65–76.

485 Kendrick, M.A., Scambelluri, M., Honda, M., Phillips, D. (2011) High abundances of noble
486 gas and chlorine delivered to the mantle by serpentinite subduction. Nat. Geosci. 4, 807-812.

487 Kendrick, M.A., Woodhead, J.D., and Kamenetsky, V.S. (2012). Tracking halogens through
488 the subduction cycle. Geology *40*, 1075–1078.

489 Kendrick, M.A., Jackson, M.G., Hauri, E.H., Phillips (2015). The halogen (F, Cl, Br, I) and
490 H_2O systematics of Samoan lavas: Assimilated-seawater, EM2 and high- $^3He/^4He$
491 components. Earth and Planet. Sci. Lett. 410, 197-209.
492
493 Kovalenko, V.I., Naumov, V.B., Girnis, A.V., Dorofeeva, V.A., and Yarmolyuk, V.V. (2006).
494 Composition and chemical structure of oceanic mantle plumes. Petrology *14*, 452–476.

495 Marty, B., Yokochi, R., (2006). Water in the Early Earth. Reviews in Mineralogy and
496 Geochemistry 62, 421-450.
497
498 Marty, B. (2012). The origins and concentrations of water, carbon, nitrogen and noble gases on
499 Earth. Earth Planet. Sci. Lett. *313-314*, 56–66.

500 Mayer, M., 1997. SIMNRA User's Guide. Report IPP 9/113, Max-Planck-Institut für
501 Plasmaphysik, Garching, Germany.

502 McDonough, W.F., and Sun, S. -s. (1995). The composition of the Earth. Chem. Geol. *120*,
503 223–253.

504 Metrich, N., and Rutherford, M. (1992). Experimental-Study of Chlorine Behavior in Hydrous
505 Silicic Melts. Geochim. Cosmochim. Acta *56*, 607–616.

506 Ottolini, L.P., and Fèvre, B.L. (2008). SIMS analysis of chlorine in metasomatised upper-
507 mantle rocks. Microchim. Acta *161*, 329–336.

508 Pagé, L., Hattori, K., de Hoog, J.C.M., Okay, A.I. (2016). Halogen (F, Cl, Br, I) bahaviour in
509 subducting slabs: a study in lawsonite blueshist in Western Turkey. Earth and Planet. Sci. Let.
510 442, 133-142.
511
512 Pearson, D.G., Brenker, F.E., Nestola, F., McNeill, J., Nasdala, L., Hutchison, M.T., Matveev,
513 S., Mather, K., Silversmit, G., Schmitz, S., et al. (2014). Hydrous mantle transition zone
514 indicated by ringwoodite included within diamond. Nature *507*, 221–224.

515 Philippot, P., Agrinier, P., and Scambelluri, M. (1998). Chlorine cycling during subduction of
516 altered oceanic crust. Earth Planet. Sci. Lett. *161*, 33–44.

517 Pyle D. M. and Mather T. A., 2009. Halogens in igneous processes and their fluxes to the
518 atmosphere and oceans from volcanic activity: A review, Chem. Geol., vol. 263, n° 1-4, p. 110-
519 121.

520 Ringwood, A.E. (1975). Composition and Petrology of the Earth's Mantle. McGraw-Hill *New
521 York*.

522 Roberge, M., Bureau, H., Bolfan-Casanova, N., Frost, D.J., Raepsaet, C., Surblé, S., Khodja,
523 H., Auzende, A.L. , Fiquet, G. (2015). Is the the transition zone a deep reservoir for fluorine?
524 Earth and planet. Sci. Lett. 429, 25-32.

525 Rocholl, A.B.E., Simon, K., Jochum, K.P., Bruhn, F., Gehann, R., Kramar, U., Luecke, W.,
526 Molzahn, M., Pernicka, E., Seufert, M., et al. (1997). Chemical Characterisation of NIST
527 Silicate Glass Certified Reference Material SRM 610 by ICP-MS, TIMS, LIMS, SSMS, INAA,
528 AAS and PIXE. Geostand. Newsl. *21*, 101–114.

529 Rudnick R.L., Gao S. (2003). Composition of the continental crust. Treatrise on Geochemistry

530 3: 1-64.

531 Rubin, A.E., and Choi, B.-G. (2009). Origin of Halogens and Nitrogen in Enstatite Chondrites.
532 Earth Moon Planets *105*, 41–53.

533 Saal, A.E., Hauri, E.H., Langmuir, C.H., and Perfit, M.R. (2002). Vapour undersaturation in
534 primitive mid-ocean-ridge basalt and the volatile content of Earth's upper mantle. Nature *419*,
535 451–455.

536 Scambelluri, M., Müntener, O., Ottolini, L., Pettke, T.T., and Vannucci, R. (2004). The fate of
537 B, Cl and Li in the subducted oceanic mantle and in the antigorite breakdown fluids. Earth
538 Planet. Sci. Lett. *222*, 217–234.

539 Sharp, Z.D., Draper, D.S. (2013) The Chlorine abundance of the Earth: Implications for a
540 habitable planet. Earth and Planet. Sci. Lett. 369, 71-77.
541
542 Schmandt, B., S. D., Jacobsen, T. W., Becker, Z. X., Liu, K. G,. Dueker, 2014. Dehydration
543 melting at the top of the lower mantle. Science, 344, 1265-1268.

544 Stalder, R., Kronz, A., and Simon, K. (2008). Hydrogen incorporation in enstatite in the system
545 MgO–SiO$_2$–H$_2$O–NaCl. Contrib. Mineral. Petrol. *156*, 653–659.

546 Straub, S.M., and Layne, G.D. (2003). The systematics of chlorine, fluorine, and water in Izu
547 arc front volcanic rocks: Implications for volatile recycling in subduction zones. Geochim.
548 Cosmochim. Acta *67*, 4179–4203.

549 Tatsumi Y. (1989). Migration of fluid phases and genesis of basalt magmas in subduction zones.
550 J. Geophys. Res. 94, 4697-4707.
551
552 Toffelmier, D.A., and Tyburczy, J.A. (2007). Electromagnetic detection of a 410-km-deep melt
553 layer in the southwestern United States. Nature, 447, 991-994.
554
555 Weiss Y., Kiflawi I., Davies N., Navon O. (2014), High-density fluids and the growth of
556 monocrystalline diamonds. *Geochimica et Cosmochimica Acta* 141, 145-159.
557
558 Withers, A.C., Bureau, H., Raepsaet, C., and Hirschmann, M.M. (2012). Calibration of infrared
559 spectroscopy by elastic recoil detection analysis of H in synthetic olivine. Chem. Geol. *334*,
560 92–98.

561

562

Figure captions
564

565 **Figure 1:**
566 Sample #S5553 (1100°C and 20 GPa): hydrous Cl-bearing ringwoodite synthesized at 1100°C and 20
567 GPa.
568 A. PIXE spectrum of one Rw crystal Cl and Fe Kalpha and Kbeta rays respectively at 2.62 – 2.81 and
569 6.40 – 7.05 KeV are labelled on the spectrum.
570 B. SEM photography of sample #S5553. Ringwoodite (in light grey), the largest grain sizes are of more
571 than 70 µm; stishovite is not present on this section, a Cl-rich melt is visible in grain boundaries. The
572 white square is corresponding to the total map analysed with PIXE.
573 C. PIXE elemental map for iron.
574 D. PIXE elemental map for Cl.
575 A pure ringwoodite crystal is selected using the combination of the SEM photography with the elemental
576 compositions (e.g. iron C and chlorine D) in order to avoid any chemical contamination from intersticial
577 melt. This crystal is represented by the black shape in the SEM photography, and by the white shape in
578 the chemical maps C and D. This area of interest (one ringwoodite crystal) is used to generate the PIXE
579 spectrum presented in A.
580

581 **Figure 2:**
582 SEM photography of A) S5551 (anhydrous Cl-bearing ringwoodite synthesized at 1100°C and 20 GPa).
583 Rw ringwoodite (in light grey), the grain sizes are of about 15 µm; St stishovite crystals are in dark grey
584 with 6 µm medium size, intergranular glass is dark B) H3697 (hydrous Cl-bearing ringwoodite
585 synthesized at 1400°C and 22 GPa), Rw ringwoodite (in light grey), the grain sizes are of about 20 µm;
586 St stishovite crystals are in dark grey, intergranular glass is dark.
587

588

589 **Figure 3**
590 TEM analysis of a ringwoodite thin section of about 100 nm thickness (prepared by focused ion beam)
591 for transmission electron microscopy study, from sample #S5553 (20 GPa, 1100°C, 240 min.)
592 containing 99 ppm wt. Cl and 4766 ppm wt. H_2O.
593 A: Scanning Transmission Electron Microscopy (STEM) bright field micrograph of the ringwoodite
594 showing the only heterogeneities found in the sample.
595 B and C: EDX analysis of Na and Cl contents within the green rectangle in A (1800 x 1100 nm^2), they
596 show that heterogeneities are not related to any Cl-rich or NaCl-rich inclusions, and emphasize the
597 uniform distribution.
598

599 **Figure 4:**
600 Cl content in ppm wt. versus temperature in °C. No significant effect of the temperature on the Cl content
601 is seen.
602 Legend: white squares: hydrous wadsleyite, white triangles: hydrous ringwoodite. black triangle:
603 anhydrous ringwoodite.
604

605 **Figure 5:**
606 Cl content in ppm wt. versus water contents in ppm wt. The highest Cl concentration is corresponding
607 to anhydrous ringwoodite. Cl content seems to slightly decrease with water content, but we notice that
608 for a same Cl content of about 100 ppm wt., the water content is ranging from 932 to 4766 ppm in
609 ringwoodite. It would mean that the Cl content is not affected by water for such low amounts.
610 Same legend than Fig 4.
611

612 **Figure 6:**
613

614 Cl and F concentrations measured in Wd and Rw, synthesized using the same experimental protocol and
615 from NaCl and NaF sources. Data from this study and from Roberge et al. (2015). Assuming a hydrous
616 transition zone, ranges of potential Cl and F concentrations in Ol, Wd, Rw are proposed.

617   Legend: white squares: hydrous wadsleyite, white triangles: hydrous ringwoodite, white circles:
618   olivines, black triangles: anhydrous ringwoodite, black square: anhydrous wadsleyite.
619
620
621   **Figure 7**
622
623   State of the art of the Cl and F budgets of the Earth, assuming a continuous supply by subduction of the
624   TZ with respect to Cl and F. Reservoirs: crust (Rudnick and Gao, 2003); upper mantle without TZ (Saal,
625   2002); TZ, Cl this study, F (Rogerge et al., 2015); lower mantle, Cl (Beyer et al., 2012), F (Kovalenko
626   et al., 2006). Degassing Fluxes are expressed in HCl (4.3 10^{12} g/yr) and HF (0.5 10^{12} g/yr), they are
627   corresponding to 4.18 10^{12} g/yr Cl and 0.47 10^{12} g/yr F respectively, data are from Pyle and Mather
628   (2009); subducted fluxes are from Straub and Layne (2003) and John et al. (2011).
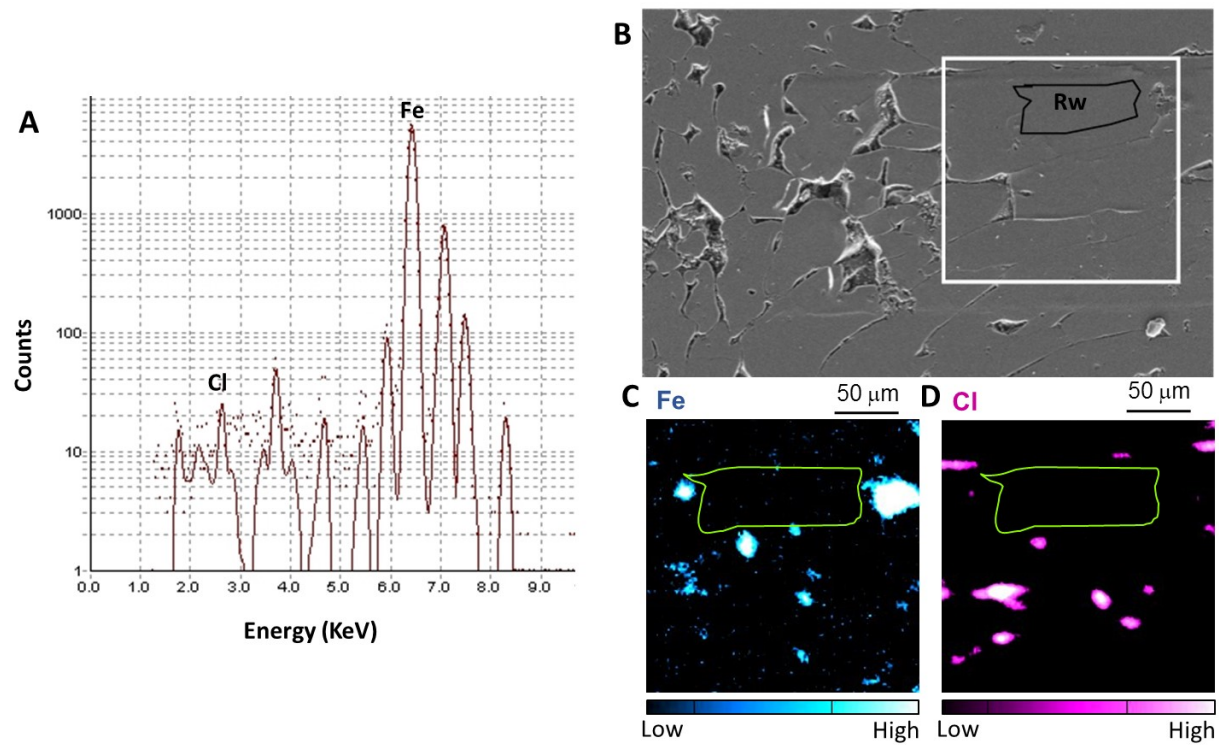629
630
631
632

633 **Figure 1:**

634

635
636
637
638
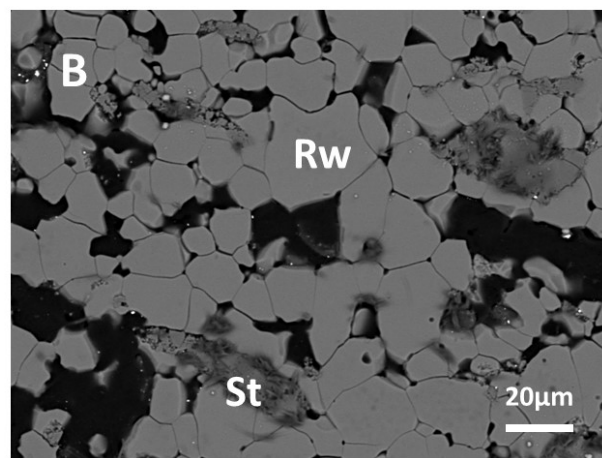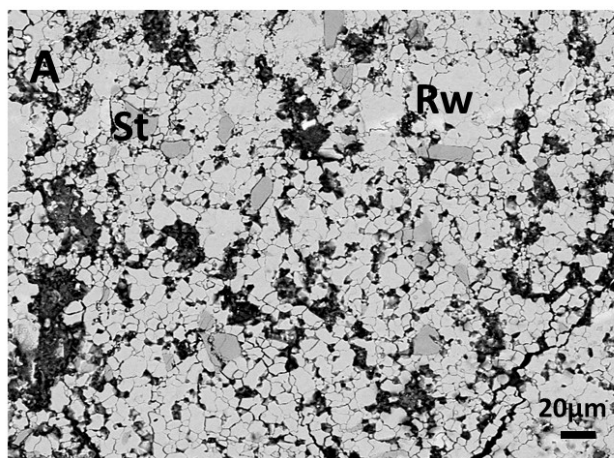
Figure 2:

654　　**Figure 3:**
655
656
657

658
659

660   **Figure 4:**

661

662
663
664
665
666
667
668
669
670
671
672
673

674 **Figure 5:**

675
676

677

Figure 6:

681
682
683
684
685
686
687
688
689
690
691
692
693
694
695
696
697
698
699
700
701
702
703
704

705

706 **Figure 7**

707

708

Atmosphere

HF 0.5 (±0.2) 10^{12}g/yr (1)
HCl 4.3 (±1) 10^{12}g/yr (1)

Global
Subduction

Crust

240 ppm Cl   550 ppm F

Global
Degassing   1 ppm Cl 1.14×10^{22}g F   16 ppm F
             6.78×10^{20}g Cl

                                            $9.9\text{-}10 \times 10^{12}$g F/yr
                                            $2{,}9\text{-}22 \times 10^{12}$g Cl/yr

Upper Mantle

80 ppm Cl 16.8×10^{22}g F   460 ppm F
             3×10^{22}g Cl   TZ

21 ppm Cl 3.85×10^{22}g F   12 ppm F
             6.27×10^{22}g Cl

Lower Mantle

709

710

711

712

713

714

715

716

717

718

719

720   **Table 1:** Starting materials, experimental conditions and sample descriptions.

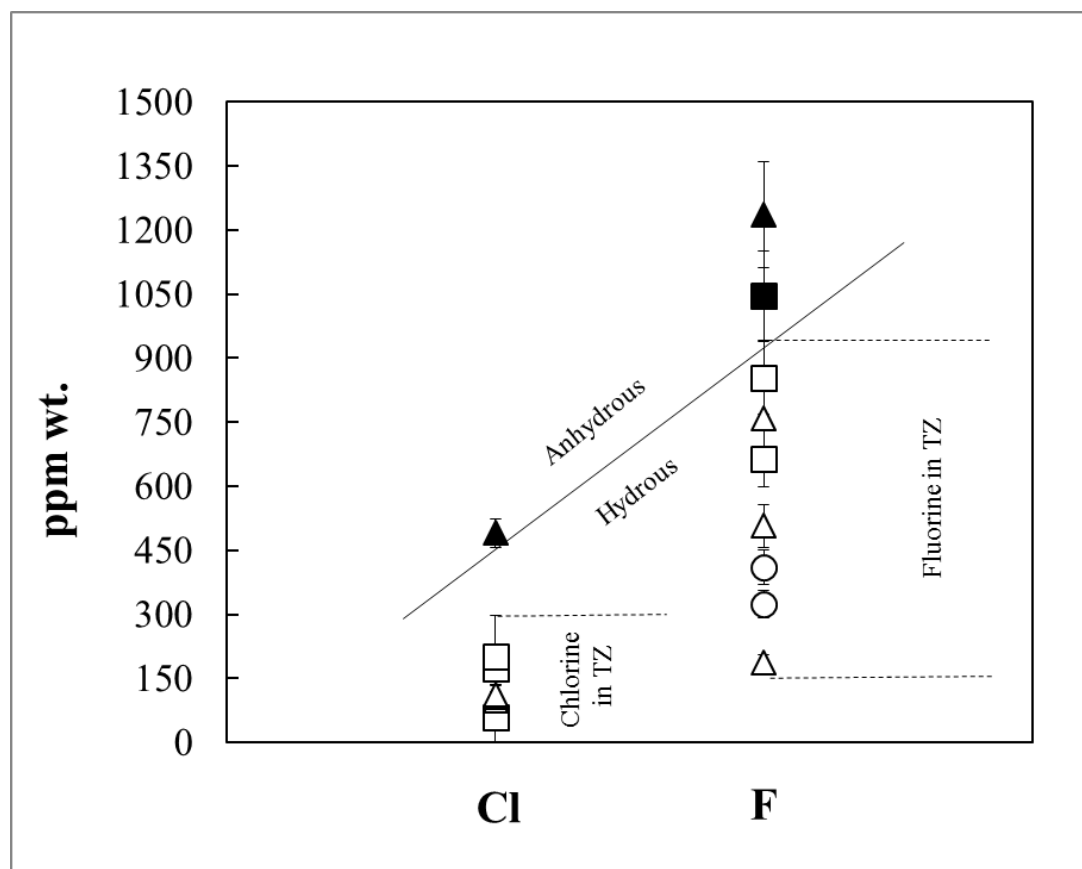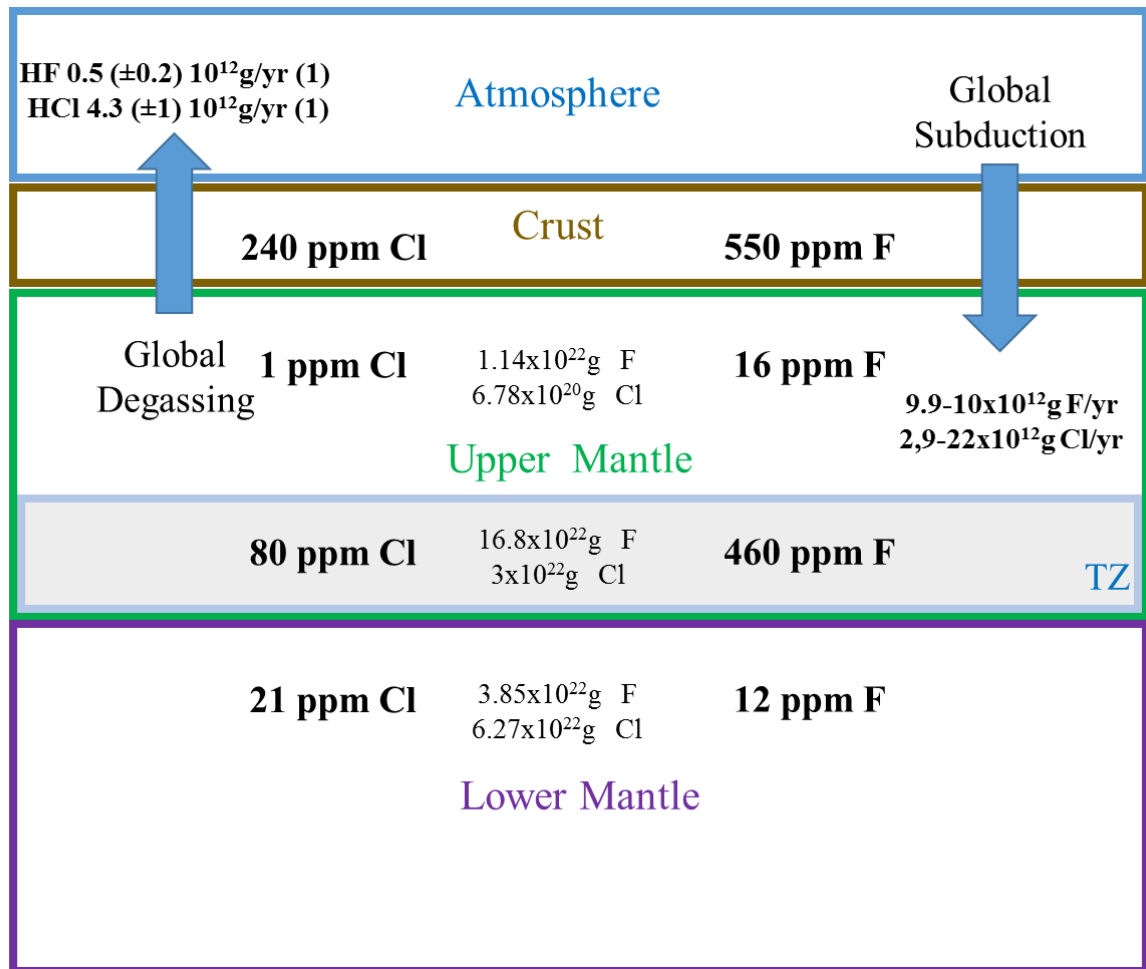| Sample	P (GPa)	T (°C)	Time (min)	Starting material	Phases
References					
83(*)	15	1400	20	Pure SC	Wadsleyite (>400 µm)
H3698(*)	22	1400	20	Pure SC	Ringwoodite (>400 µm)
Anhydrous					
87_Cl(*)	14	1350	420	SCP + 5wt.% NaCl + 2 wt.% Mg(OH)$_2$	Wadsleyite (20 µm) Enstatite NaCl-glass
S5551(**)	20	1100	240	SCP + 5wt.% NaCl + 2 wt.% Mg(OH)$_2$	Ringwoodite(40 µm) Stishovite (10 µm) NaCl-glass
Hydrous					
40_Cl(*)	14	1100	240	SP + 5wt.% NaCl + 2 wt.% Mg(OH)$_2$	Wadsleyite (40 µm) Enstatite NaCl-glass
86(*)	15	1250	540	SCP + 5wt.% NaCl + 2 wt.% Mg(OH)$_2$	Wadsleyite (30 µm) Enstatite (10 µm) NaCl-glass
88_Cl(*)	14	1400	360	SCP + 5wt.% NaCl + 2 wt.% Mg(OH)$_2$	Wadsleyite (70 µm) Enstatite (10 µm) NaCl-glass
S5553(***)	20	1100	240	SCP + 5wt.% NaCl + 2 wt.% Mg(OH)$_2$	Ringwoodite (>200 µm) stishovite(15 µm) NaCl-glass
H3694(*)	22	1250	240	SCP + 5wt.% NaCl + 2 wt.% Mg(OH)$_2$	Ringwoodite (100 µm) Stishovite (20 µm) NaCl-glass
H3697(*)	22	1400	240	SCP + 5wt.% NaCl + 2 wt.% Mg(OH)$_2$	Ringwoodite (> 300µm) Stishovite (20 µm) NaCl-glass

721   SC San Carlos olivine, SCP San Carlos olivine powder + SiO$_2$; SP synthetic powder of SiO$_2$ + MgO +
722   FeO; (*) Au-Pd capsule, (**) Re capsule, (***) Pt capsule, NaCl pure salt, Mg(OH)$_2$ brucite, Larger grain
723   sizes are given in brackets when measured.

724

28

725 **Table 2:** Representative analyses of wadsleyites and ringwoodites. Major elements are from EPMA, Cl from PIXE, H_2O from ERDA.
726 Wd= wadsleyite, Rw =ringwoodite, Nb =number of EPMA analysis, Mg#=Mg/(Fe+Mg) ratio atomic, (Fe+Mg)/SiO_2 atomic ratio. Error in brackets is the standard deviation
727 for EPMA analysis and is in (%) for PIXE and ERDA.

728

Sample	P ± 1GPa	T ±50°C	Time min	Phase	Oxydes (%wt)									Nb	Mg#	(Mg+Fe)/Si	(ppm)	
					SiO_2	FeO	MnO	Al_2O_3	Na_2O	MgO	CaO	TiO_2	Total				H_2O	Cl
Reference																		
83	15	1400	20	Wd	41.55 (0.09)	9.21 (0.10)	0.12 (0.04)	0.11 (0.02)	0.02 (0.02)	48.48 (0.29)	0.02 (0.03)	0.01 (0.01)	99.63 (0.38)	9	0.90	1.92		
H3698	22	1400	20	Rw	41.50 (0.31)	9.70 (0.14)	0.12 (0.05)	0.04 (0.04)	0.01 (0.01)	48.79 (0.27)	0.07 (0.02)	0.01 (0.02)	100.39 (0.38)	14	0.90	1.95		
Anhydrous																		
87_Cl	14	1350	420	Wd	41.38 (0.39)	8.56 (0.16)	0.08 (0.03)	0.07 (0.02)	0.16 (0.03)	48.87 (0.42)	0.03 (0.03)	0.03 (0.02)	99.18 (0.21)	7	0.91	1.93		ND
S5551	20	1100	240	Rw	41.40 (0.86)	9.00 (0.33)	0.14 (0.04)	0.05 (0.03)	0.06 (0.04)	47.84 (0.93)	0.04 (0.01)	0.01 (0.01)	98.54 (0.29)	4	0.90	1.91		490 (33)
Hydrous																		
40_Cl	14	1100	240	Wd	41.13 (0.34)	8.84 (0.20)	0.02 (0.02)	0.24 (0.04)	0.22 (0.05)	49.09 (0.52)	0.02 (0.01)	0.02 (0.03)	99.58 (0.75)	6	0.91	1.96	917 (15)	174 (22)
86	15	1250	540	Wd	41.49 (0.46)	8.57 (0.13)	0.09 (0.03)	0.08 (0.01)	0.19 (0.03)	48.88 (0.34)	0.00 (0.00)	0.02 (0.02)	99.32 (0.47)	6	0.91	1.93	1659 (14)	60 (60)
88_Cl	14	1400	360	Wd	41.55 (0.20)	8.04 (0.20)	0.05 (0.03)	0.09 (0.02)	0.19 (0.02)	49.65 (0.24)	0.01 (0.01)	0.02 (0.02)	99.6 (0.35)	6	0.92	1.94	1115 (14)	200 (48)
S5553	20	1100	240	Rw	41.63 (0.22)	7.63 (0.13)	0.07 (0.03)	0.03 (0.02)	0.04 (0.01)	49.42 (0.04)	0.00 (0.00)	0.02 (0.02)	98.84 (0.42)	3	0.92	1.92	4766 (13)	99 (12)
H3694	22	1250	240	Rw	40.49 (0.55)	7.67 (0.07)	0.04 (0.04)	0.07 (0.00)	0.09 (0.04)	49.97 (0.42)	0.00 (0.01)	0.03 (0.02)	98.36 (0.30)	3	0.92	2.00	932 (14)	106 (26)
H3697	22	1400	240	Rw	41.37 (0.37)	8.18 (0.34)	0.07 (0.02)	0.06 (0.02)	0.10 (0.05)	49.57 (0.35)	0.01 (0.01)	0.02 (0.02)	99.38 (0.29)	7	0.92	1.95	1554 (13)	113 (20)

729

730

731